ACS APPLIED MATERIALS & INTERFACES

Research Article

www.acsami.org

Synergistic Effect of Double-Shelled and Sandwiched TiO_2@Au@C Hollow Spheres with Enhanced Visible-Light-Driven Photocatalytic Activity

Jiabai Cai,[†,§] Xueqing Wu,[†,§] Shunxing Li,*[,†,‡] Fengying Zheng,[†,‡] Licong Zhu,[†] and Zhanghua Lai[†]

[†]College of Chemistry and Environment, Minnan Normal University, Zhangzhou 363000, P. R. China

[‡]Fujian Province Key Laboratory of Modern Analytical Science and Separation Technology, Minnan Normal University, Zhangzhou, 363000, P. R. China

Ⓢ *Supporting Information*

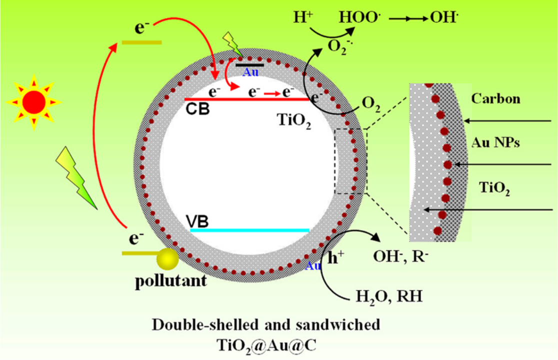

ABSTRACT: A novel approach for the fabrication of double-shelled, sandwiched, and nanostructured hollow spheres was proposed, using hydrotherm reaction and calcination. The negatively charged nanoparticles (e.g., Au, Ag, and Pt) could be adsorbed successively onto the positively charged hollow spheres (e.g., TiO_2, ZnO, and ZrO_2). The resulted nanocomposites (TiO_2@Au, as a proof-of-concept) were dispersed in glucose solution under hydrothermal conditions. After calcination, uniform double-shelled and sandwiched TiO_2@Au@C hollow spheres were obtained and Au nanoparticles were sandwiched between the shell wall of TiO_2 and C. The samples were characterized by SEM, TEM, XRD, XPS, BET, and UV−vis DRS. The photocatalytic activity for the degradation of 4-nitroaniline was in the order of TiO_2@Au@C > TiO_2@C > TiO_2/Au > P25. The visible-light photodegradation rate of 92.65% for 4-nitroaniline was achieved by TiO_2@Au@C, which exhibited an increase of 75% compared to Degussa P25 TiO_2. Furthermore, no deactivation occurred during catalytic reaction for three times, i.e., the TiO_2@Au@C microspheres exhibited superior photocatalytic stability. TiO_2@Au@C microspheres could also enhance the photocatalytic activity for hydrogen generation from methanol/water solutions. The synergistic effect of coupling TiO_2 hollow spheres with Au nanoparticles and C shell on photocatalytic performance was proved by us. The photoexcited electrons from Au nanoparticles could be captured by the conduction band of TiO_2 and then the electron−hole separation was improved. Moreover, both the visible light absorption and the affinity between TiO_2 and pollutants could be improved by the coexistence of carbonaceous materials, which could facilitate the photocatalytic interface reaction.

KEYWORDS: *double-shell sandwiched nanomaterials, sunlight, photodegradation, hydrogen production*

1. INTRODUCTION

Over the past several years, sunlight-driven photocatalysis has been considered as an environment-friendly and efficient method for aromatic pollutants removal[1−3] and the production of clean and renewable hydrogen through water splitting.[4] In the design of nanocomposite-based photocatalysts, the major obstacles should be overcome, including electron−hole separation,[5] light residence time in/on the photocatalyst,[6,7] and the affinity between pollutants and photocatalyst.[8] Such challenges can be unlocked by the innovation of the structure and morphology of the photocatalyst.[9−11] As an effective structure, hollow sphere has been used for solving the first two obstacles.[12,13] Because of the unique physical and chemical properties (e.g., large surface area, low density, and highly efficient light-harvesting ability[14]), hollow spheres of metal oxides have attracted much attention because of their wide variety of applications, including drug release systems,[15] heterogeneous catalysts,[16] waste removal,[17] the protection of light-sensitive molecules,[18] and so on.

Recently, inorganic oxide supported Au catalysts have been used for the photodegradation of organic pollutants.[19,20] Unfortunately, the supported Au catalysts with small sizes are generally unstable against thermal sintering and growing[21] so the catalytic activity of the supported Au catalysts decays rapidly. To avoid migration and aggregation of Au nanoparticles (NPs), three kinds of strategies have been developed, including the replacement of monocomponent Au NPs with Au-based alloy NPs[22] or hydroxyapatite composite,[23] the confinement of Au NPs within mesoporous supports,[24] and the encapsulation of Au NPs into core−shelled microspheres.[25] Compared with the former two methods, the last one is a more effective way, because the structure of core−shell has high thermal stability[26] and recyclability.[27] Among organic capping agents, carbonaceous materials have received particular

Received: December 4, 2014
Accepted: January 27, 2015
Published: January 27, 2015

DOI: 10.1021/am508554t
ACS Appl. Mater. Interfaces 2015, 7, 3764−3772

Scheme 1. Fabrication Process for Double-Shelled and Sandwiched TiO_2@Au@C Hollow Spheres

attention, because of their advantages in visible-light absorption and organic pollutants adsorption, which can facilitate the photocatalytic reaction. Both TiO_2@carbon with dyad structure and hierarchical TiO_2@C hybrid hollow spheres exhibit an enhanced photocatalytic efficiency for visible-light photo-oxidation.[28,29] Among the various inorganic oxides, including TiO_2,[30−32] CeO_2,[33] ZnO,[34] and ZrO_2,[35] TiO_2 with a suitable band gap of 3.2 eV is proven to be the most widely used metal oxide-based photocatalyst, because of its high photocatalytic activity, wide band gap, cost-effectivity, low toxicity, and excellent chemical stability. Despite good electronic conductivity of the carbon layer, the electron−hole recombination following excitation is still a challenge. Therefore, tailored nanostructures offer a new way for achieving this goal by facilitating electron−hole separation.

Herein, we design a general hydrothermal method to synthesize double-shelled and sandwiched TiO_2@Au@C hollow sphere, using TiO_2 hollow sphere as the template (Scheme 1 and Figure 1a). As a neutral surfactant, glucose has been used for its nonpolar long carbon chain to control the growth of the nanocrystals. Our objective is to (a) offer a new way for facilitating electron−hole separation, using the Schottky barrier junctions of TiO_2 with Au (Scheme 2), (b) enhance the light-harvesting efficiency and mass transfer through the unique hierarchical mesoporous structure, (c) increase the accessible surface area of TiO_2, and (d) improve the affinity between photocatalyst and organic pollutants through carbon layer.

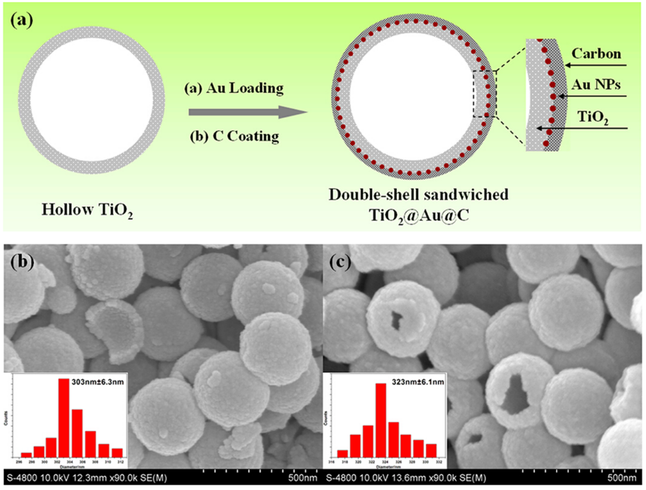

Figure 1. (a) Schematic of the fabrication process for double-shelled and sandwiched TiO_2@Au@C hollow spheres. SEM images of (b) pristine TiO_2 hollow spheres (303 nm) and (c) double-shelled and sandwiched TiO_2@Au@C hollow spheres (323 nm).

Scheme 2. Charge Transfer in Monodisperse Double-Shelled and Sandwiched TiO_2@Au@C Hollow Spheres

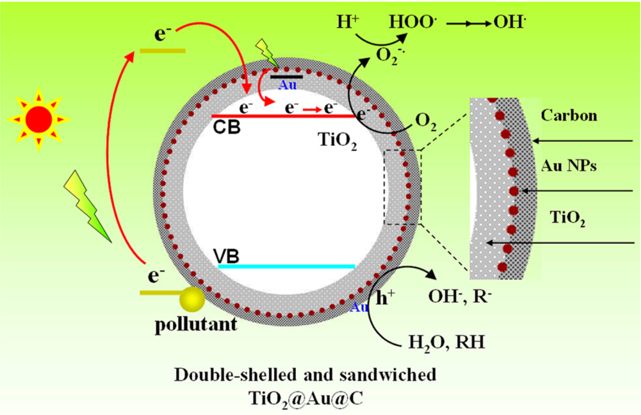

2. EXPERIMENTAL SECTION

2.1. Reagents and Chemicals. Tetrabutyl titanate (TBOT, J&K, 99%), tetrachloroauric (III) acid hydrate ($AuCl_3 \cdot HCl \cdot 4H_2O$, Sinopharm, 99%), trisodium citrate dihydrate ($C_6H_{12}O_7Na_3 \cdot 2H_2O$, Xilong, 99%), D-glucose ($C_6H_{12}O_6 \cdot H_2O$, Xilong), and ethanol (C_2H_5OH, Xilong, 99.7%) were purchased in China and used without further purification. Distilled water was employed as the polymerization medium.

2.2. Synthesis of Au Nanoparticle.[36] An aqueous solution of $HAuCl_4 \cdot 3H_2O$ (0.1 wt %, 10 mL) was added to deionized water (100 mL) and heated to boiling point. A sodium citrate solution (1 wt %, 2 mL) was then added and the resulting mixture was kept for 15 min under stirring. Upon cooling to room temperature, the Au NPs were separated from the solution by centrifugation and redispersed in water (10 mL).

2.3. Synthesis of Monodisperse Polystyrene Spheres. The monodisperse polystyrene (PS) spheres were prepared by the interpolymerization of methyl acrylate and styrene, according to a modified method.[37] The reactor used included a double-neck round-bottom flask, mechanical agitation, temperature controller, reflux condenser, and N_2 agitation. After replacing the air inside the reactor with N_2, the reaction system was kept under N_2 until the polymerization was completed. After adding distilled water (85 mL), styrene (10.47 mL), and methyl acrylate (0.52 mL), the reactor was heated and kept at 70 °C. $Na_2S_2O_8$ solution (30 g/L, 5 mL) was added to start the polymerization process for 24 h, and then PS latex (ca. 10% solid content) was collected and used as templates.

2.4. Synthesis of TiO_2 Hollow Spheres. TBOT (0.18 mL) was dissolved in ethanol (10 mL), in which 0.25 g of PS dispersed in the mixture of water (0.15 mL) and ethanol (72 mL) was added. After refluxing at 80 °C for 4 h, the obtained PS@TiO_2 nanocomposite was washed three times with ethanol, dried in vacuum at 60 °C for 6 h, heated with a rate of 5 °C/min, and maintained at 550 °C (i.e., calcination temperature) for 3 h to remove the PS core. Single-shelled TiO_2 hollow spheres were finally obtained.

2.5. Synthesis of TiO_2/Au Hollow Spheres. The prepared Au NPs in aqueous solution (3 mL) were mixed with water (30 mL) and this mixture was stirred for 10 min at room temperature. Subsequently, hollow TiO_2 (0.05 g) was added and the resulting mixture was kept for

10 h under stirring. The resultant solid product was centrifuged, washed three times with ethanol, and dried in vacuum at 60 °C for 6 h.

2.6. Synthesis of TiO_2@C Hollow Spheres. Glucose (1 g) was mixed with water (30 mL) and the reaction mixture was stirred for 30 min at room temperature. Subsequently, hollow TiO_2 (0.05g) was added and the resulting mixture was kept for 30 min under stirring. The mixture was transferred to Teflon-lined stainless steel autoclaves and heated to 180 °C for 3 h. TiO_2@C composite particles were obtained after centrifugation and washing procedures.

2.7. Synthesis of TiO_2@Au@C Hollow Spheres. Hollow TiO_2 was mixed with water (30 mL) and the reaction mixture was stirred for 30 min at room temperature. Subsequently, the prepared Au NPs in aqueous solution (3 mL) were added and the resulting mixture was kept for 30 min under stirring. Glucose (1 g) was added and stirred for another 30 min at room temperature. The mixture was transferred to Teflon-lined stainless steel autoclaves and heated to 180 °C for 3 h. The obtained TiO_2@Au@C particles were washed by centrifugation/redispersion cycles with ethanol for three times and dried in vacuum at 60 °C for 6 h. Finally, the spontaneously formed carbon shells were used as the stern layers to generate double-shelled and sandwiched TiO_2@Au@C hollow spheres through calcination in argon atmosphere.

2.8. Characterization. After being coated with a thin Pt layer, the samples were tested by a Gemini microscope (Hitachi, S-4800, Japan) at an accelerating voltage of 10 kV to obtain their scanning electron microscopy (SEM) images. Transmission electron microscopy (TEM) was conducted on a Tecnai G2 F20 U-TWIN (FEI, USA) under the acceleration voltage of 200 kV. Samples for TEM were prepared by drying a drop of dilute nanocomposite suspension on a carbon grid. Samples were also analyzed by energy dispersive X-ray spectroscopy (EDX) on the same TEM to disclose the independent existence of C shell and TiO_2 shell, i.e., double-shell in TiO_2@Au@C hollow spheres. Structural properties of the nanocomposite were investigated by X-ray diffraction (XRD, D/MAX-TTRIII(CBO), Rigaku Corporation, Japan) patterns with monochromatic Cu $K\alpha$ radiation (40 kV, 30 mA) in the range of 20°−80°. After being mixed with KBr, the samples were measured by a Thermo Nicolet FT-IR iS10 spectrometer (USA) and then Fourier-transform infrared (FTIR) spectra were obtained. The nanocomposite was dried in a vacuum for 12 h and then its thermogravimetric analysis (TG) was carried out a TG 2009F1 analyzer (NETZSCH, Germany) in the range of 25−900 °C at a heating rate of 15 K/min under nitrogen atmosphere. Fine $BaSO_4$ powder was used as a standard for the baseline, and the UV−vis absorption spectra of TiO_2, TiO_2/Au, TiO_2@C, and TiO_2@Au@C hollow spheres were recorded on a UV−vis 2550 spectrophotometer (Shimadzu). X-ray photoelectron spectroscopy (XPS, Thermal Scientific K-Alpha XPS spectrometer) was used to investigate the distribution of Ti, Au, and C in TiO_2@Au@C hollow spheres. Using an ASAP2020 instrument, BET surface area was determined via N_2 adsorption at 77 K over a relative pressure (P/P_0) range from 0.01 to 0.99.

2.9. Photocatalytic Activity Measurements. The photocatalysts (30 mg of P25, TiO_2, TiO_2/Au, TiO_2@C, or TiO_2@Au@C) with aromatic pollutant (4-nitroaniline or 4-nitrophenol, 5×10^{-3} g/L) were stirred in the dark for 1 h, and the adsorption/desorption equilibrium between pollutants and hollow spheres was reached. The photocatalytic performance was then tested under visible light irradiation at room temperature. A Xenon Short Arc Lamp (350 W) was used as light source, and the irradiation spectrum was cut off below 420 nm using a Pyrex glass for the simulation of sunlight.[38] After photodegradation for different time intervals, the samples were taken out of the aqueous dispersions, the photocatalysts were removed by filtration, and the pollutant concentration was determined by spectrophotometry. The degradation rate was calculated using eq 1.

$$\text{Degradation rate} = 100\% \times (C_0 - C)/C_0 \tag{1}$$

Here, C_0 and C are the concentrations of the pollutant in the solution before and after visible light irradiation, respectively.

The first-order kinetic equation (eq 2) was used to fit the experimental data:

$$\ln(C_0/C) = k_{app} \times t \tag{2}$$

where k_{app} is the reaction rate constant and t is the reaction time.[39]

3. RESULTS AND DISCUSSION

3.1. Morphology and Structure of the Double-Shelled and Sandwiched TiO_2@Au@C Hollow Spheres. Aligned, double-shelled, and sandwiched TiO_2@Au@C hollow spheres were prepared on the template of TiO_2 hollow spheres by a one-step hydrothermal process (Experimental Section). In our work, the well-defined hollow TiO_2 submicrospheres could be easily obtained via a seed-assisted high-temperature calcination method, according to our previous work (Figure 1b).[40] In the pH range of 2−5, the outer layers of TiO_2 hollow spheres had positive surface charges (seen in Supporting Information (SI) Figure S1),[40] which could enhance the affinity between TiO_2 and gold sol (negatively charged)[41] by electrostatic adsorption, and then the surface coverage and adsorption rate of Au NPs onto the TiO_2 hollow spheres were increased. Meanwhile, TiO_2@Au hollow spheres could be prepared by this electrostatic adsorption process. Under high temperature and high pressure of hydrothermal treatment, the condensation of glucose in solution led to the formation of amorphous carbon shell, in which the Au NPs were located in the sandwich layer. After calcination in argon atmosphere, the spontaneously formed carbon shells were used as the stern layers to generate double-shelled and sandwiched TiO_2@Au@C hollow spheres. The surface morphology and size distribution of TiO_2 and TiO_2@Au@C hollow spheres are shown in Figure 1b and 1c, respectively. After coating Au NPs and C shell onto TiO_2 shell, the diameter of hollow spheres was increased from 303 to 323 nm. A smooth carbon shell was formed on the TiO_2 surface by a glucose-assisted hydrothermal method (for details, see SI Figures S2 and S3). The photocatalytic activity for the degradation of 4-nitroaniline was in the order of TiO_2@Au@C > TiO_2@C > TiO_2/Au > P25. The visible-light photodegradation rate of 92.65% by TiO_2@Au@C was achieved, which exhibited a 75% increase compared to Degussa P25 TiO_2, because a Schottky barrier was assumed to form at the TiO_2−Au interface and the TiO_2 conduction band as electron sink could reduce the recombination of photoinduced electrons and holes. This result was similar to that of Au@TiO_2 core−shell hollow spheres.[42]

In agreement with the SEM data (Figure 1c), the TEM images (Figure 2a) revealed that the produced TiO_2@Au@C were hollow and porous. A close inspection of the TEM image of TiO_2@Au@C hollow spheres (Figure 2c) revealed the presence of individual nanoparticles on a thick and layered shell. The morphology and structure of TiO_2, TiO_2/Au, TiO_2@C, and TiO_2@Au@C hollow spheres was characterized by SEM and TEM (SI Figure S4). The HRTEM image of the nanocomposite showed three types of intimately contacted lattice fringes, confirming the formation of the junctions between TiO_2, Au, and C (Figure 2b). The lattice spacing of 0.351 nm was the interplanar distance between adjacent (101) crystallographic planes of TiO_2, while the lattice spacing of 0.24 nm matched that of the (111) plane of Au NPs. Furthermore, the coated carbon layer with a thickness of ca. 10 nm (Figure 2b) created a smooth, highly conductive layer over the entire nanospheres surface. The polycrystalline nature of these individual nanoparticles was also confirmed by the SAED measurements (Figure 2d). Several important features could be recognized. The prepared microspheres had rather uniform

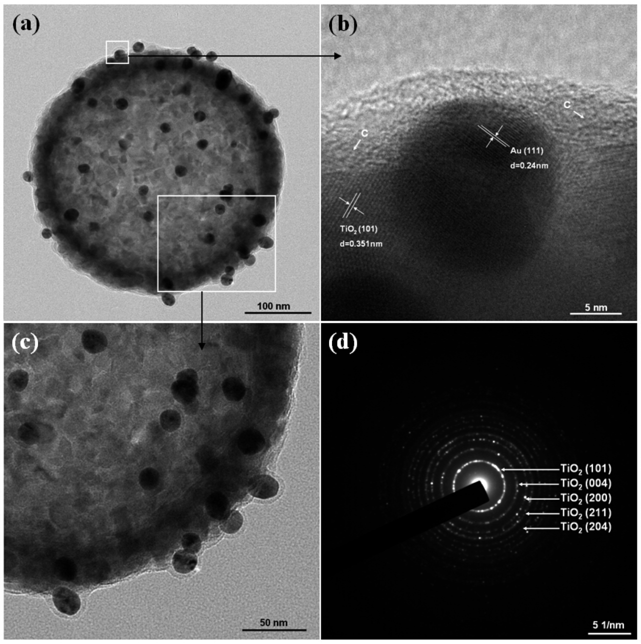

Figure 2. TEM (a and c), HRTEM (b), and SAED (d) images of double-shelled and sandwiched TiO_2@Au@C hollow spheres.

diameters of 323 nm (Figure1c). By changing the volume of added Au NPs (3, 1.5, 1, or 0.5 mL), the content of Au NPs on the microspheres could be tuned (SI Figure S5). The diameter of Au NPs in the sandwich layer was about 16−20 nm (SI Figure S6). The HRTEM image further indicated that each Au NPs was highly crystalline with the interplanar spacing of 0.24 nm, corresponding to the (111) planes of Au NPs. It was noted that the lattice spacing of Au NPs could not be changed clearly due to hydrothermal and calcination process (Figure 2c). In our system, the well-defined hollow microspheres were easily obtained in the presence of gold sol. A plausible explanation was that gold sol could accelerate the formation process of TiO_2@Au@C solid microspheres. Meanwhile, the thickness of C shell could be easily adjusted by changing the quantity of glucose (1, 2, 3, or 4 g) in the reaction mixture (SI Figures S7 and S8).

The hollow spheres of TiO_2, TiO_2/Au and TiO_2@Au@C were investigated by XRD analysis and the results are shown in Figure 3. Six peaks of TiO_2 were found at 2θ = 25.22, 37.78, 47.94, 54.15, 54.96, and 62.69, which were indexed to the (101), (004), (200), (211), (105), and (204) planes of TiO_2, respectively, and these results were in good agreement with the standard pattern of anatase (JCPDS 21-1272). The diffraction peaks of TiO_2/Au microspheres had a consistent position with pure TiO_2 submicrospheres. The constant peak position indicated the phase structure of TiO_2 had not been changed during the Au coating process. Furthermore, the Au coating process did not provide any structural or morphological transformations as demonstrated by SEM and TEM results (Figures 1 and 2, respectively). Interestingly, after the second layer-by-layer deposition (i.e., carbon coating), the XRD pattern of TiO_2@Au@C still only demonstrated the characteristic of anatase TiO_2 phase, because partial carbon atoms from TiO_2@Au@C existed in an amorphous phase and the content of carbon was so limited that strong diffraction peaks could not be observed.

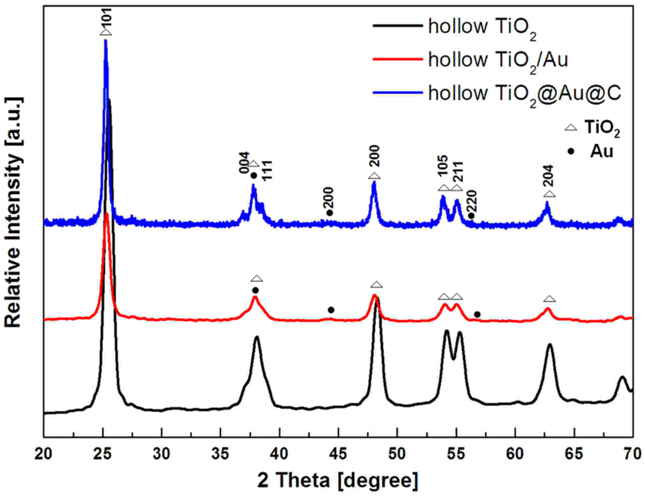

Figure 3. XRD pattern of TiO_2, TiO_2/Au, and double-shelled and sandwiched TiO_2@Au@C hollow spheres.

The full range XPS spectrum of TiO_2@Au@C hollow spheres is shown in Figure 4a. The XPS peaks of Ti $2p_{3/2}$ and $2p_{1/2}$ were located at about 458.5 and 464.2 eV with a good symmetry (Figure 4b), indicating that the chemical valence of Ti was +4 in octahedral coordination with oxygen.[29] Moreover, the chemical environments for Ti and O_L were not changed, strongly suggesting that carbon and nitrogen originated from TBOT did not enter the TiO_2 crystal lattice under the mild solvothermal conditions. The XPS spectra of TiO_2@Au@C (Figure 4c) show the peaks of Au $4f_{7/2}$ and Au $4f_{5/2}$ centered at 84.2 and 87.8 eV, respectively. The spin energy separation of 3.6 eV was in good agreement with reported data of Au $4f_{7/2}$ and Au $4f_{5/2}$ in Au NPs.[36] Figure 4d shows the C 1s peak from XPS, which corresponded to the carbon layers in the TiO_2@Au@C hollow spheres. No obvious peaks were detected around 281.5 and 283 eV, indicating that the carbon originated from glucose was not doped into the TiO_2 lattice.

The diffuse reflectance UV−vis spectra of the prepared photocatalysts are shown in Figure 5. The UV absorption band at ∼400 nm, corresponding to the band gap of 3.2 eV,[43] could be attributed to the band-edge absorption of anatase TiO_2.[44] After coating C shell onto hollow TiO_2 and hollow TiO_2/Au, their absorbances in the region of 300−400 nm were affected by the band absorption of the amorphous carbon (shown in Figure 5). The absorption features from 360 to 600 nm arose from the band absorption of the amorphous carbon.[45] The absorption of Au NPs and amorphous carbon was in the range of 500−600 nm[36] and 360−600 nm, respectively. Their absorption spectra were seriously overlapping. Furthermore, in the TiO_2@Au@C hollow spheres, the content of C was higher than that of Au, and the absorption of C was stronger than that of Au. No obvious difference in the UV−vis spectra between TiO_2@C and TiO_2@Au@C was observed. The light absorption of TiO_2@Au@C hollow spheres was stronger than that of TiO_2 hollow sphere in sunlight light region (Figure 5), i.e., the visible-light harvesting efficiency of TiO_2@Au@C hollow spheres was improved.

Besides high photostability and excellent water-solubility, low cytotoxicity was important for TiO_2@Au@C hollow spheres as safe nanomaterials. The cytotoxicity of TiO_2@Au@C hollow spheres was evaluated using a standard cell viability assay (i.e., 3-[4,5-dimethylthiazol-2-yl]-2,5-diphenyltetrazolium bromide

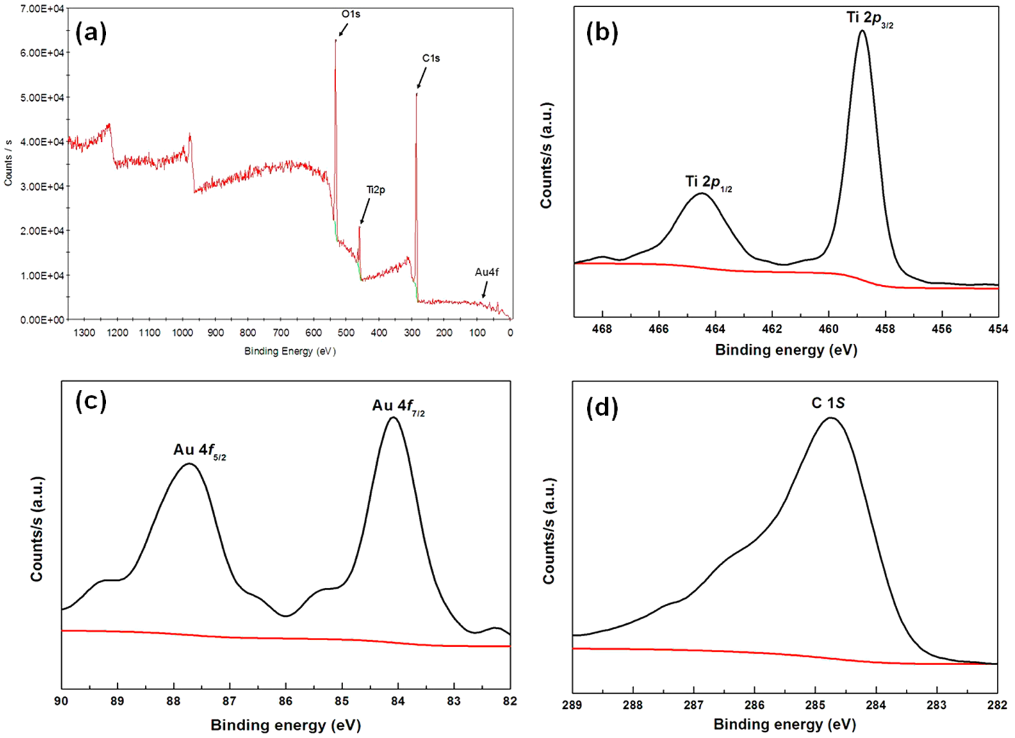

Figure 4. Full range of the XPS spectrum (a), XPS peaks of Ti 2p (b), Au 4f (c), and C 1s (d) of double-shelled and sandwiched TiO_2@Au@C hollow spheres.

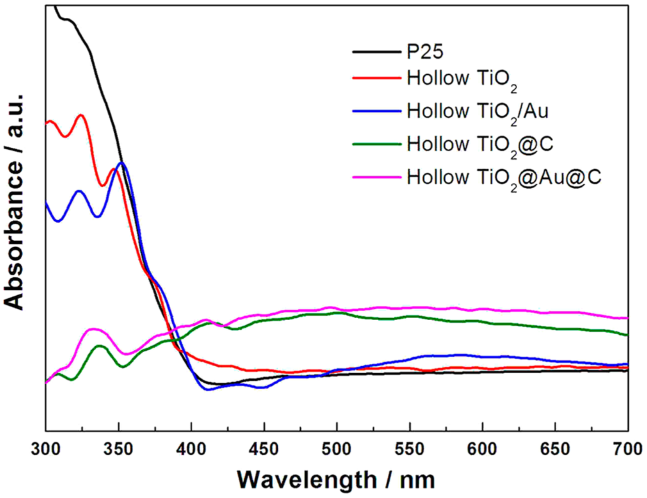

Figure 5. Diffuse reflectance UV−vis spectra of P25, TiO_2, TiO_2/Au, TiO_2@C, and double-shelled and sandwiched TiO_2@Au@C hollow spheres (the 500−600 nm is gold plasmonic band).

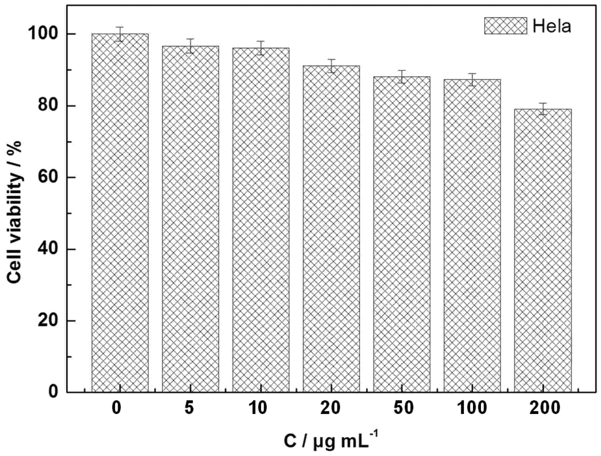

Figure 6. HeLa cell viability after incubating with double-shelled and sandwiched TiO_2@Au@C hollow spheres for 24 h and quantitative assays by standard MTT method.

(MTT) assay). HeLa cells exposed to TiO_2@Au@C with different concentrations (0−200 μg mL^{-1}) for 24 h and the influence of TiO_2@Au@C concentrations on cell viability was tested. As shown in Figure 6, 79.12% of HeLa cells retained viability after being exposed to 200 μg mL^{-1} of TiO_2@Au@C. The form of HeLa cell was not so much obviously changed (SI Figure S10). Even at the highest concentration tested (200 μg mL^{-1}), the cytotoxicity of TiO_2@Au@C was not significant in our MTT assay, which implied that the double-shelled and sandwiched TiO_2@Au@C hollow spheres were lowly toxic and environmentally friendly.

3.2. Evaluation of Photocatalytic Activity. To investigate the influence of the photocatalyst structure on catalytic activity, five kinds of photocatalysts, including P25, hollow TiO_2, hollow TiO_2@C, hollow TiO_2/Au, and double-shelled and sandwiched TiO_2@Au@C hollow spheres, were used for the photodegradation of 4-nitroaniline and 4-nitrophenol under simulated sunlight irradiation for 180 min. The results are shown in Figure 7. Only 17.61% of 4-nitroaniline could be photodegraded by P25. The photocatalytic activity of TiO_2@Au@C was higher than that of P25, TiO_2, TiO_2@C, and TiO_2/Au. The photodegradation rate of 4-nitroaniline by TiO_2@Au@C was 92.65%. Meanwhile, the linear relationship between $\ln(C_0/C)$ and t indicated that the photodegradation reactions followed pseudo-first-order kinetics (Figure 7) with rate constants (0.0012, 0.0004, 0.0050, 0.0046, and 0.015 min^{-1}) and correlation coefficients R^2 (0.987, 0.987, 0.999, 0.995, and

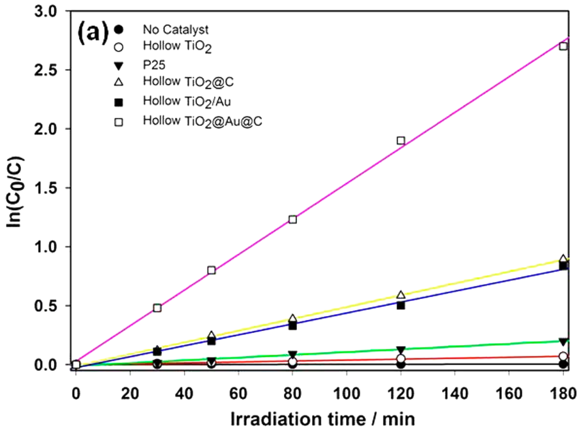

Figure 7. Linear transform $\ln(C_0/C) = f(t)$ of the kinetic curves of (a) 4-nitroaniline or (b) 4-nitrophenol photodegradation by P25, hollow TiO_2, hollow TiO_2@C, hollow TiO_2/Au, and double-shelled and sandwiched TiO_2@Au@C hollow spheres under visible light irradiation.

0.999) for P25, TiO_2, TiO_2@C, TiO_2/Au, and TiO_2@Au@C, respectively. For comparison, the same procedure was also performed for 4-nitrophenol (Figure 7, Table 1, and SI Table S1). The relative photocatalytic activity of photocatalysts for aromatic pollutant degradation was in the order of TiO_2@Au@C > TiO_2@C > TiO_2/Au > P25. The photocatalytic performance of hollow TiO_2 was improved by the coupling of Au and C (Figure 7 and Table 1). This synergistic effect could be attributed to the following reasons. After coating carbon shell onto TiO_2 hollow spheres, the affinity between photocatalyst and aromatic pollutants could be improved. Compared with TiO_2 hollow spheres, the adsorption ratio of TiO_2@Au@C for 4-nitroaniline and 4-nitrophenol in 60 min was increased 1.13% and 5.80%, respectively (Figure 8). Certainly, the surface coverage of aromatic pollutants on the TiO_2@Au@C was more than that on TiO_2 hollow spheres. Energy could be transferred from aromatic pollutants to the TiO_2 conduction band. The back electron could also be transferred from Au NPs to the TiO_2 conduction band. The photodegradation rate of 4-nitroaniline was used as a measure of the efficiency of these prepared nanocatalysts in producing •OH radicals. The visible-light photodegradation rate of TiO_2@Au@C was 92.65%, which exhibited a 30% increase compared with TiO_2@C. The electron–hole separation could be facilitated through the unique hierarchically mesoporous structure. On the other hand, a Schottky barrier was assumed to form at the TiO_2–Au interface, and the TiO_2 conduction band as electron sink could reduce the recombination of photo-induced electrons and holes. The N_2 gas has been used by us to remove the oxygen in the water and the photodegradation rate was reduced (SI Figure S11). The result indicated that the photocatalytic activity of TiO_2@Au@C could be suppressed by the decrease of oxygen concentration. This result proved that the •OH radicals, which were mainly depending on the electron-transfer mediation, played an important role in the photocatalysis process. The specific surface area, pore volume, and average pore size of TiO_2@Au@C hollow spheres were

Table 1. Visible Light Photodegradation Rate Constant k (min^{-1}) for P25, TiO_2, TiO_2@C, TiO_2/Au, and Double-Shelled and Sandwiched TiO_2@Au@C Hollow Spheres

	k (min^{-1})	
sample	4-nitroaniline	4-nitrophenol
P25	0.0012	0.0009
hollow TiO_2	0.0004	0.0014
hollow TiO_2@C	0.0050	0.0036
hollow TiO_2/Au	0.0046	0.0033
double-shelled and sandwiched TiO_2@Au@C	0.015	0.0081

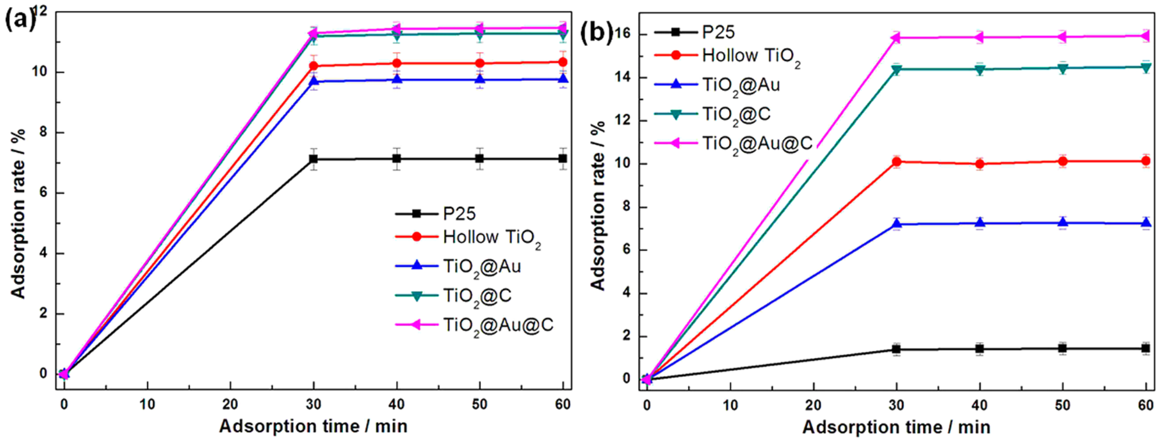

Figure 8. Adsorption rate of (a) 4-nitroaniline and (b) 4-nitrophenol on P25, hollow TiO_2, hollow TiO_2@C, hollow TiO_2/Au, and double-shelled and sandwiched TiO_2@Au@C hollow spheres under dark.

62.95 m^2 g^{-1}, 0.1452 cm^3 g^{-1}, and 1.352 nm, respectively (SI Figure S12 and Table S2), indicating TiO_2@Au@C hollow spheres were also typical mesoporous materials. The stability of TiO_2@Au@C was examined by the degradation of 4-nitroaniline during a three-cycle experiment. After three cycles, the photocatalytic activity decreased slightly, which indicated that TiO_2@Au@C exhibited good photocatalytic stability (SI Figure S13). After three cycles experiment of photodegradation, the hollow structure of TiO_2@Au@C still remained, which indicated that the structure stability and mechanical strength of TiO_2@Au@C were good (SI Figure S14).

The time vs hydrogen production for as-prepared samples is shown in Figure 9. Under irradiation with the light beam ($\lambda \geq$ 420 nm), the values of hydrogen production rate constant (r_{H2}, obtained as the slope of the linear part of the curves in Figure 9 and SI Figure S15) are collected in Table 2 and Table 3. Under visible light irradiation, the hydrogen production rate of double-shelled and sandwiched TiO_2@1.43%Au@C hollow spheres was 319.5 μmol h^{-1} g^{-1} at first hour, which was higher than that of P25 (Table 2). The hydrogen production rate was found to be fairly linear with light irradiation time from 1.0 to 5.0 h. We also tested the P25, hollow TiO_2, and hollow TiO_2@C for photocatalytic hydrogen production at the same conditions, and no hydrogen could be determined. The improvement on the photocatalytic hydrogen production activity might be due to the fast separation of the photoinduced electron/hole pairs for the stability of Au NPs.[4,46,47]

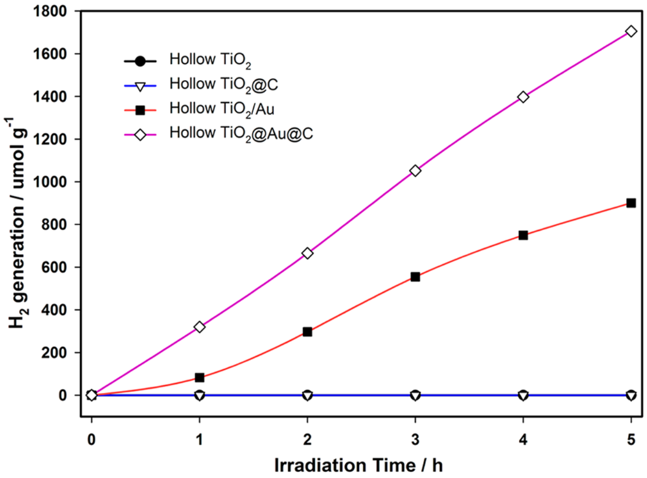

Figure 9. Visible-light photocatalytic hydrogen generation by hollow TiO_2, hollow TiO_2/Au, hollow TiO_2@C, and double-shelled and sandwiched TiO_2@1.43%Au@C hollow spheres in methanol−water system.

Table 2. Hydrogen Production Rate (r_{H2}) in the Visible-Light Photocatalytic Splitting of Methanol−Water System

sample	r_{H2} (μmol h^{-1} g^{-1})	relative rate
P25	0	
hollow TiO_2	0	
hollow TiO_2@C	0	
hollow TiO_2/Au	193.2	1
double-shelled and sandwiched TiO_2@1.43% Au@C	347.1	1.8

Table 3. Hydrogen Production Rate (r_{H2}) in the Visible-Light Photocatalytic Splitting of Methanol−Water System

sample	r_{H2} (μmol h^{-1} g^{-1})
hollow TiO_2@7.29%Au@C	60.0
hollow TiO_2@4.04%Au@C	192.7
hollow TiO_2@1.43%Au@C	347.1
hollow TiO_2@0.65%Au@C	182.9

The reaction pathway (R1) was as follows:

$$CH_3OH \rightarrow H_2 + CH_2O \quad (R1)$$

Reaction 1 was a multistep reaction:

$$Au + hv \rightarrow e^- + h^+ \quad (R1a)$$

$$CH_3OH + 2h^+ \xrightarrow{Au} CH_2O + 2H^+ \quad (R1b)$$

$$2H^+ + 2e^- \rightarrow H_2 \quad (R1c)$$

The role of Au was important, because photoexcited electrons from Au NPs could be trapped by the TiO_2 conduction band and some of them were subsequently transferred to hydrogen ions (Scheme 3).[48,49] By changing the volume of added Au NPs (3, 1.5, 1, or 0.5 mL), the content of Au NPs on the microspheres could be tuned (SI Figure S5). The hydrogen production rates of TiO_2@Au@C with different contents of Au NPs are listed in SI Figure S15. The hydrogen production rates of TiO_2@Au@C were different with different contents of Au NPs. The hydrogen production rate of TiO_2@1.43%Au@C was the highest, i.e, 1.43% was the optimal content of Au NPs in TiO_2@Au@C. A further increase in Au loading (i.e., more than 1.43%) could lead to the increase of Au particle size (SI Figure S5) and resulted in the decrease of photocatalytic hydrogen production rate (Table 3). This decrease could be attributed to a reduction in the available metal−support sites where both metal and support were needed for the reaction to occur.[48]

Scheme 3. Mechanism of Methanol Photocleavage over Photogenerated Electrons (e^-) and Holes (h^+) Migration to TiO_2 and Au of the Monodisperse Double-Shelled and Sandwiched TiO_2@Au@C Hollow Spheres

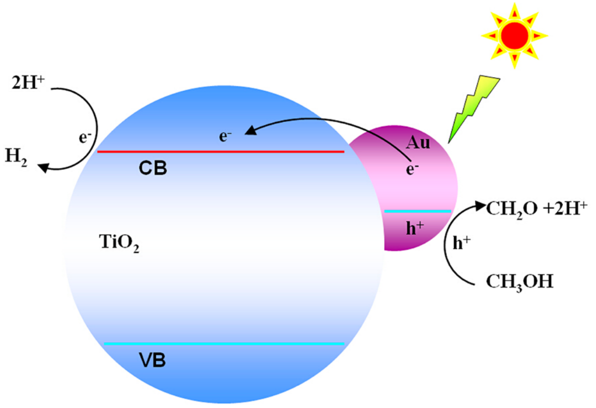

4. CONCLUSIONS

In summary, we proposed a simple approach for the fabrication of TiO_2@Au@C hollow spheres and other heterojunction nanocomposites (e.g., TiO_2@Ag@C, TiO_2@Pt@C, ZnO@Au@C, ZnO@Ag@C, ZnO@Pt@C, etc.) with uniform double-shelled and sandwiched structure, which could be used for environmental cleanup.

■ ASSOCIATED CONTENT

Ⓢ Supporting Information

SEM and TEM images, XRD pattern, EDX data, TG data, FTIR spectra, nitrogen adsorption−desorption isotherm, surface area, and porosity measurements of TiO_2@Au@C hollow spheres, correlation coefficient R^2. This material is available free of charge via the Internet at http://pubs.acs.org/.

■ AUTHOR INFORMATION

Corresponding Author

*Tel.: +86 596 2591395. Fax: +86 596 2591395. E-mail: lishunxing@mnnu.edu.cn.

Author Contributions

§Xueqing Wu and Jiabai Cai contributed equally to this work.

Notes

The authors declare no competing financial interest.

■ ACKNOWLEDGMENTS

This work is supported by the National Natural Science Foundation of China (21175115 and 21475055, S.X.L), the Program for New Century Excellent Talents in University (NCET-11 0904, S.X.L), and the Science & Technology Committee of Fujian Province, China (2012Y0065, F.Y.Z).

■ REFERENCES

(1) Xu, X.; Randorn, C.; Efstathiou, P.; Irvine, J. T. A Red Metallic Oxide Photocatalyst. *Nat. Mater.* **2012**, *11*, 595−598.

(2) Shannon, M. A.; Bohn, P. W.; Elimelech, M.; Georgiadis, J. G.; Marinas, B. J.; Mayes, A. M. Science and Technology for Water Purification in the Coming Decades. *Nature* **2008**, *452*, 301−310.

(3) Yoon, T. P.; Ischay, M. A.; Du, J. Visible Light Photocatalysis as a Greener Approach to Photochemical Synthesis. *Nat. Chem.* **2010**, *2*, 527−532.

(4) Rosseler, O.; Shankar, M. V.; Du, M. K.-L.; Schmidlin, L.; Keller, N.; Keller, V. Solar Light Photocatalytic Hydrogen Production from Water over Pt and Au/TiO_2 (Anatase/Rutile) Photocatalysts: Influence of Noble Metal and Porogen Promotion. *J. Catal.* **2010**, *269*, 179−190.

(5) Li, R.; Zhang, F.; Wang, D.; Yang, J.; Li, M.; Zhu, J.; Zhou, X.; Han, H.; Li, C. Spatial Separation of Photogenerated Electrons and Holes Among {010} and {110} Crystal Facets of $BiVO_4$. *Nat. Commun.* **2013**, *4*, 1432.

(6) Mubeen, S.; Lee, J.; Singh, N.; Krämer, S.; Stucky, G. D.; Moskovits, M. An Autonomous Photosynthetic Device in which all Charge Carriers Derive from Surface Plasmons. *Nat. Nanotechnol.* **2013**, *8*, 247−251.

(7) Chen, W.; Fan, Z.; Zhang, B.; Ma, G.; Takanabe, K.; Zhang, X.; Lai, Z. Enhanced Visible-Light Activity of Titania Via Confinement Inside Carbon Nanotubes. *J. Am. Chem. Soc.* **2011**, *133*, 14896−14899.

(8) Li, S.-X.; Cai, S.-J.; Zheng, F.-Y. Self Assembled TiO_2 with 5-Sulfosalicylic Acid for Improvement Its Surface Properties and Photodegradation Activity of Dye. *Dyes Pigm.* **2012**, *95*, 188−193.

(9) Zhang, H.; Lv, X.; Li, Y.; Wang, Y.; Li, J. P25-Graphene Composite as a High Performance Photocatalyst. *ACS Nano* **2009**, *4*, 380−386.

(10) Zhang, J.; Xu, Q.; Feng, Z.; Li, M.; Li, C. Importance of the Relationship Between Surface Phases and Photocatalytic Activity of TiO_2. *Angew. Chem., Int. Ed.* **2008**, *47*, 1766−1769.

(11) Varghese, O. K.; Paulose, M.; LaTempa, T. J.; Grimes, C. A. High-Rate Solar Photocatalytic Conversion of CO_2 and Water Vapor to Hydrocarbon Fuels. *Nano Lett.* **2009**, *9*, 731−737.

(12) Jing, L.; Zhou, W.; Tian, G.; Fu, H. Surface Tuning for Oxide-Based Nanomaterials as Efficient Photocatalysts. *Chem. Soc. Rev.* **2013**, *42*, 9509−9549.

(13) Li, S.; Chen, J.; Zheng, F.; Li, Y.; Huang, F. Synthesis of the Double-Shell Anatase-Rutile TiO_2 Hollow Spheres with Enhanced Photocatalytic Activity. *Nanoscale* **2013**, *5*, 12150−12155.

(14) Hu, J.; Chen, M.; Fang, X.; Wu, L. Fabrication and Application of Inorganic Hollow Spheres. *Chem. Soc. Rev.* **2011**, *40*, 5472−5491.

(15) Zhu, Y.; Kockrick, E.; Ikoma, T.; Hanagata, N.; Kaskel, S. An Efficient Route to Rattle-Type Fe_3O_4@SiO_2 Hollow Mesoporous Spheres Using Colloidal Carbon Spheres Templates. *Chem. Mater.* **2009**, *21*, 2547−2553.

(16) Li, X.; Huang, R.; Hu, Y.; Chen, Y.; Liu, W.; Yuan, R.; Li, Z. A Templated Method to Bi_2WO_6 Hollow Microspheres and Their Conversion to Double-Shell Bi_2O_3/Bi_2WO_6 Hollow Microspheres with Improved Photocatalytic Performance. *Inorg. Chem.* **2012**, *51*, 6245−6250.

(17) Cao, J.; Zhu, Y.; Bao, K.; Shi, L.; Liu, S.; Qian, Y. Microscale Mn_2O_3 Hollow Structures: Sphere, Cube, Ellipsoid, Dumbbell, and Their Phenol Adsorption Properties. *J. Phys. Chem. C* **2009**, *113*, 17755−17760.

(18) Li, S.; Zheng, J.; Chen, D.; Wu, Y.; Zhang, W.; Zheng, F.; Cao, J.; Ma, H.; Liu, Y. Yolk-Shell Hybrid Nanoparticles with Magnetic and pH-Sensitive Properties for Controlled Anticancer Drug Delivery. *Nanoscale* **2013**, *5*, 11718−11724.

(19) Heutz, N. A.; Dolcet, P.; Birkner, A.; Casarin, M.; Merz, K.; Gialanella, S.; Gross, S. Inorganic Chemistry in a Nanoreactor: Au/TiO_2 Nanocomposites by Photolysis of a Single-Source Precursor in Miniemulsion. *Nanoscale* **2013**, *5*, 10534−10541.

(20) Ayati, A.; Ahmadpour, A.; Bamoharram, F. F.; Tanhaei, B.; Mänttäri, M.; Sillanpää, M. A Review on Catalytic Applications of Au/TiO_2 Nanoparticles in the Removal of Water Pollutant. *Chemosphere* **2014**, *107*, 163−174.

(21) Li, W.-C.; Comotti, M.; Schüth, F. Highly Reproducible Syntheses of Active Au/TiO_2 Catalysts for CO Oxidation by Deposition-Precipitation or Impregnation. *J. Catal.* **2006**, *237*, 190−196.

(22) Liu, X.; Wang, A.; Wang, X.; Mou, C.-Y.; Zhang, T. Au-Cu Alloy Nanoparticles Confined in SBA-15 as a Highly Efficient Catalyst for CO Oxidation. *Chem. Commun.* **2008**, 3187−3189.

(23) Zhao, K.; Qiao, B.; Wang, J.; Zhang, Y.; Zhang, T. A Highly Active and Sintering-Resistant Au/FeO_x-Hydroxyapatite Catalyst for CO Oxidation. *Chem. Commun.* **2011**, *47*, 1779−1781.

(24) Chen, C.; Nan, C.; Wang, D.; Su, Q.; Duan, H.; Liu, X.; Zhang, L.; Chu, D.; Song, W.; Peng, Q. Mesoporous Multicomponent Nanocomposite Colloidal Spheres: Ideal High-Temperature Stable Model Catalysts. *Angew. Chem., Int. Ed.* **2011**, *123*, 3809−3813.

(25) Cargnello, M.; Wieder, N. L.; Montini, T.; Gorte, R. J.; Fornasiero, P. Synthesis of Dispersible Pd@CeO_2 Core-Shell Nanostructures by Self-Assembly. *J. Am. Chem. Soc.* **2009**, *132*, 1402−1409.

(26) Arnal, P. M.; Comotti, M.; Schüth, F. High-Temperature-Stable Catalysts by Hollow Sphere Encapsulation. *Angew. Chem., Int. Ed.* **2006**, *118*, 8404−8407.

(27) Park, J. C.; Bang, J. U.; Lee, J.; Ko, C. H.; Song, H. Ni@SiO_2 Yolk-Shell Nanoreactor Catalysts: High Temperature Stability and Recyclability. *J. Mater. Chem.* **2010**, *20*, 1239−1246.

(28) Zhao, L.; Chen, X.; Wang, X.; Zhang, Y.; Wei, W.; Sun, Y.; Antonietti, M.; Titirici, M. M. One-Step Solvothermal Synthesis of a Carbon@TiO_2 Dyade Structure Effectively Promoting Visible-Light Photocatalysis. *Adv. Mater.* **2010**, *22*, 3317−3321.

(29) Zhuang, J.; Tian, Q.; Zhou, H.; Liu, Q.; Liu, P.; Zhong, H. Hierarchical Porous TiO_2@C Hollow Microspheres: One-Pot Synthesis and Enhanced Visible-Light Photocatalysis. *J. Mater. Chem.* **2012**, *22*, 7036−7042.

(30) Li, H.; Bian, Z.; Zhu, J.; Huo, Y.; Li, H.; Lu, Y. Mesoporous Au/TiO_2 Nanocomposites with Enhanced Photocatalytic Activity. *J. Am. Chem. Soc.* **2007**, *129*, 4538−4539.

(31) Murdoch, M.; Waterhouse, G.; Nadeem, M.; Metson, J.; Keane, M.; Howe, R.; Llorca, J.; Idriss, H. The Effect of Gold Loading and Particle Size on Photocatalytic Hydrogen Production from Ethanol over Au/TiO_2 Nanoparticles. *Nat. Chem.* **2011**, *3*, 489−492.

(32) Lee, I.; Joo, J. B.; Yin, Y.; Zaera, F. A Yolk@Shell Nanoarchitecture for Au/TiO_2 Catalysts. *Angew. Chem., Int. Ed.* **2011**, *123*, 10390−10393.

(33) Qi, J.; Chen, J.; Li, G.; Li, S.; Gao, Y.; Tang, Z. Facile Synthesis of Core-Shell Au@CeO_2 Nanocomposites with Remarkably Enhanced Catalytic Activity for CO Oxidation. *Energy Environ. Sci.* **2012**, *5*, 8937−8941.

(34) He, W.; Kim, H.-K.; Wamer, W. G.; Melka, D.; Callahan, J. H.; Yin, J.-J. Photogenerated Charge Carriers and Reactive Oxygen Species in ZnO/Au Hybrid Nanostructures with Enhanced Photocatalytic and Antibacterial Activity. *J. Am. Chem. Soc.* **2013**, *136*, 750−757.

(35) Wang, X.; Yu, J. C.; Chen, Y.; Wu, L.; Fu, X. ZrO_2-Modified Mesoporous Nanocrystalline $TiO_{2-x}N_x$ as Efficient Visible Light Photocatalysts. *Environ. Sci. Technol.* **2006**, *40*, 2369−2374.

(36) Daniel, M.-C.; Astruc, D. Gold Nanoparticles: Assembly, Supramolecular Chemistry, Quantum-Size-Related Properties, and Applications Toward Biology, Catalysis, and Nanotechnology. *Chem. Rev.* **2004**, *104*, 293−346.

(37) Leng, W.; Chen, M.; Zhou, S.; Wu, L. Capillary Force Induced Formation of Monodisperse Polystyrene/Silica Organic-Inorganic Hybrid Hollow Spheres. *Langmuir* **2010**, *26*, 14271−14275.

(38) Chen, Y.; Hu, C.; Hu, X.; Qu, J. Indirect Photodegradation of Amine Drugs in Aqueous Solution under Simulated Sunlight. *Environ. Sci. Technol.* **2009**, *43*, 2760−2765.

(39) Matos, J.; Laine, J.; Herrmann, J.-M. Synergy Effect in the Photocatalytic Degradation of Phenol on a Suspended Mixture of Titania and Activated Carbon. *Appl. Catal., B* **1998**, *18*, 281−291.

(40) Li, S.; Cai, J.; Wu, X.; Zheng, F.; Lin, X.; Liang, W.; Chen, J.; Zheng, J.; Lai, Z.; Chen, T. Fabrication of Positively and Negatively Charged, Double-Shelled, Nanostructured Hollow Spheres for Photodegradation of Cationic and Anionic Aromatic Pollutants under Sunlight Irradiation. *Appl. Catal., B* **2014**, *160*, 279−285.

(41) Ji, X.; Song, X.; Li, J.; Bai, Y.; Yang, W.; Peng, X. Size Control of Gold Nanocrystals in Citrate Reduction: the Third Role of Citrate. *J. Am. Chem. Soc.* **2007**, *129*, 13939−13948.

(42) Du, J.; Qi, J.; Wang, D.; Tang, Z. Facile Synthesis of Au@TiO_2 Core-Shell Hollow Spheres for Dye-Sensitized Solar Cells with Remarkably Improved Efficiency. *Energy Environ. Sci.* **2012**, *5*, 6914−6918.

(43) Abaker, M.; Dar, G.; Umar, A.; Zaidi, S.; Ibrahim, A. A.; Baskoutas, S.; Al-Hajry, A. CuO Nanocubes Based Highly-Sensitive 4-Nitrophenol Chemical Sensor. *Sci. Adv. Mater.* **2012**, *4*, 893−900.

(44) Zhang, N.; Liu, S.; Fu, X.; Xu, Y.-J. Synthesis of M@TiO_2 (M = Au, Pd, Pt) Core-Shell Nanocomposites with Tunable Photoreactivity. *J. Phys. Chem. C* **2011**, *115*, 9136−9145.

(45) Shanmugam, S.; Gabashvili, A.; Jacob, D. S.; Yu, J. C.; Gedanken, A. Synthesis and Characterization of TiO_2@C Core-Shell Composite Nanoparticles and Evaluation of Their Photocatalytic Activities. *Chem. Mater.* **2006**, *18*, 2275−2282.

(46) Fang, J.; Cao, S.-W.; Wang, Z.; Shahjamali, M. M.; Loo, S. C. J.; Barber, J.; Xue, C. Mesoporous Plasmonic Au-TiO_2 Nanocomposites for Efficient Visible-Light-Driven Photocatalytic Water Reduction. *Int. J. Hydrogen Energy* **2012**, *37*, 17853−17861.

(47) Chiarello, G. L.; Selli, E.; Forni, L. Photocatalytic Hydrogen Production over Flame Spray Pyrolysis-Synthesised TiO_2 and Au/TiO_2. *Appl. Catal., B* **2008**, *84*, 332−339.

(48) Silva, C. G.; Juarez, R.; Marino, T.; Molinari, R.; Garcıa, H. Influence of Excitation Wavelength (UV or Visible Light) on the Photocatalytic Activity of Titania Containing Gold Nanoparticles for the Generation of Hydrogen or Oxygen from Water. *J. Am. Chem. Soc.* **2011**, *133*, 595−602.

(49) Fang, C.-H.; Jia, H.-L.; Chang, S.; Ruan, Q.-F.; Wang, P.; Chen, T.; Wang, J.-F. (Gold Core)/(Titania Shell) Nanostructures forn Plasmon-Enhanced Photon Harvesting and Generation of Reactive Oxygen Species. *Energy Environ. Sci.* **2014**, *7*, 3431−3438.